Pseudo-Extensional Mode MEMS Ring Gyroscope

Igor P. Prikhodko[1], Jeffrey A. Gregory[1], Daniel Shin[2], Ryan Kwon[2], Thomas W. Kenny[2], Michael W. Judy[1]
[1]Analog Devices Inc., Wilmington, MA, USA and [2]Stanford University, Palo Alto, CA, USA

***Abstract*— This paper presents the design and characterization of a yaw gyroscope which employs a pseudo-extensional mode of a ring. The extensional mode is typically a bulk mode where the ring width expands and contracts across its circumference in contrast to a traditional wineglass mode where the in-plane ring width stays nominally constant during vibrations. Our axial symmetrical gyroscope structure is comprised of an array of concentric rings to create an apparent extensional mode, but at much lower frequency since it is made of flexural elements. An advantage inherent to the new mode is the local rejection of linear accelerations as compared to the fundamental wineglass, which rejects linear accelerations by matching electrodes across the diameter of the ring. Implemented in the wafer-level Epitaxial Silicon Encapsulation process, the device occupies an area of 1.8 mm² and initial characterization clearly demonstrates feasibility of using the pseudo-extensional mode of vibration for rate sensing with Q-factors of 110,000 and noise level of 0.06 °/√hr.**

I. Introduction

The majority of MEMS flexural ring and BAW gyroscopes with electrostatic transduction suffer from the impact of changes in electrode gaps introduced from external stresses such as thermal gradients, external shocks, mechanical stress and torque. Changes in gaps amount to changes in sensitivity (scale factor) and zero-rate offset for these sensors making them vulnerable to external vibrations. One of the solutions that commercial companies (e.g. Silicon Sensing Systems) pursued is to utilize a magnetic transduction which is more tolerant to gap changes [1], but the trade-off is the increased size and an intricate package assembly for magnet housing which drives up cost. In contrast here, we take advantage of the proposed pseudo-extensional mode of vibration with inherent vibration rejection properties while preserving a SWaP+C metric associated with the electro-statically transduced MEMS [2,3].

II. Principle of Operation

Conventional ring gyroscopes utilize wineglass vibratory modes. These modes are classified by half the number of nodes (the points of zero displacement) with the most common approach to operate the gyroscope in a fundamental, n = 2 mode. The modes with higher nodes (n = 3,4) have advantages such as tolerance to fabrication imperfections but are often overlooked because a larger node number means lower angular gain (Bryan's factor k, $0 < k \leq 1$), and hence degradation in noise performance. The previous statement, however, is only true for the modes where the ring width stays constant during vibration (e.g. conventional wineglass mode). Extensional modes of vibration are higher order modes where a ring width varies across its circumference also have n = 2,3,4 variants. Nevertheless, the n = 2 extensional mode, which is the focus of this work, should have the same angular gain k = 0.8, as the n = 2 wineglass mode. A gyroscope operation in a higher order mode without compromising the angular gain is, therefore, possible in an extensional mode.

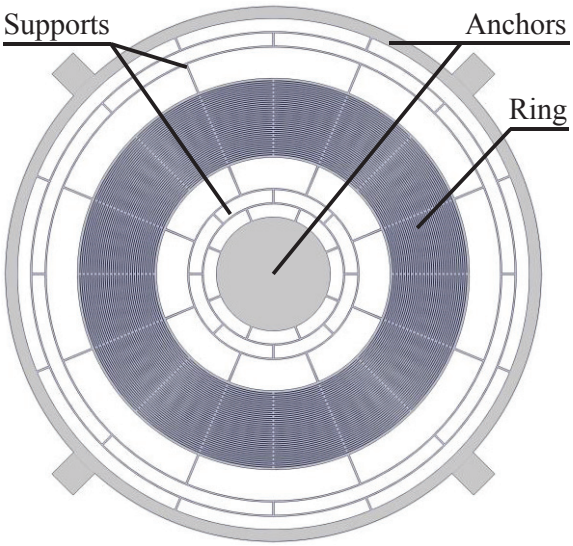

Fig. 1. Layout of the pseudo-extensional mode MEMS ring gyroscope showing composite ring, inner and outer supports and anchors (electrodes are omitted).

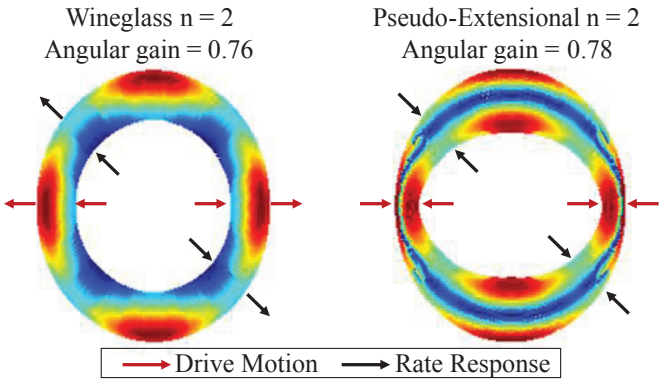

Fig. 2. FEA simulation of wineglass (left) and pseudo-extensional mode (right) showing modal displacements (anchors and supports are omitted). The angular gain of the extensional mode is the same as that of the wineglass mode.

A. Design

The presented MEMS gyroscope design consists of multiple concentric rings which act as flexural elements approximating an extensional mode, Fig. 1,2. The device consists of an outer and inner anchor supporting a composite ring and electrodes positioned on opposite sides of the ring structure, Fig. 3,4. The vibrational energy in typical axisymmetric devices operated in a wineglass mode is concentrated either at the outermost ring (e.g. Disk Resonator Gyroscope [4]) or the innermost ring (e.g. Toroidal Ring Gyroscope [5]) depending on the anchor location. In contrast, the vibrational energy of the extensional mode is concentrated roughly equally at the inner and the outer sides of a ring, providing means for a localized differential transduction when electrodes are placed on the opposite sides, see Fig. 3.

978-1-5386-7828-2/19/$31.00 ©2019 IEEE

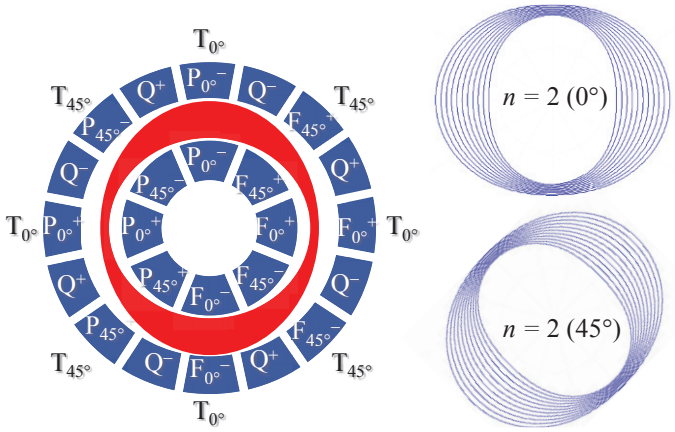

Fig. 3. Electrodes configuration for extensional mode transduction comprising 4 inner/outer forcer pairs (F), 4 pick-off pairs (P), and 8 quadrature tuning (Q). Frequency tuning electrodes (T) are shared between the forcers and pick-offs.

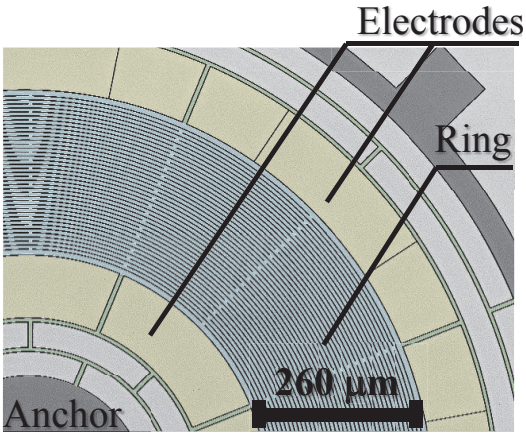

Fig. 4. Colored SEM image of the fabricated device showing a composite ring (blue), supporting structures (green), anchors (grey), and electrodes (yellow).

Note that distribution of the vibrational energy on opposite sides of a composite ring is a characteristic of the extensional mode rather than the anchors location. Fig. 1 and Table I show the layout and geometric parameters for the composite mesh ring and the supporting springs. The composite ring consists of 40 individual rings connected to each other by 8 studs with 22.5° offset in every other ring to lower the resonant frequency and increase Q-factor due to thermoelastic damping. The supporting structure [3] (shown as green in Fig. 4) ensures the vibrational energy is concentrated inside the ring and away from the anchors thus decoupling vibratory motion from a substrate and improving Q-factor due to anchor losses. As opposed to designs with single anchors [4,5], the presented device has inner and outer anchors to stiffen the translation modes which are sensitive to external vibrations thereby reducing susceptibility to shock/G-sensitivity.

B. Electrodes

The presented device can be operated in either the wineglass mode (WG) or the pseudo-extensional (PE) mode. The mode of operation of the MEMS gyroscope is selected by changing the frequency of excitation and the configuration of the electrodes. Differential vs. common-mode combinations of inner and outer electrostatic electrodes select whether the fundamental WG or PE mode is excited and sensed as shown by electrodes

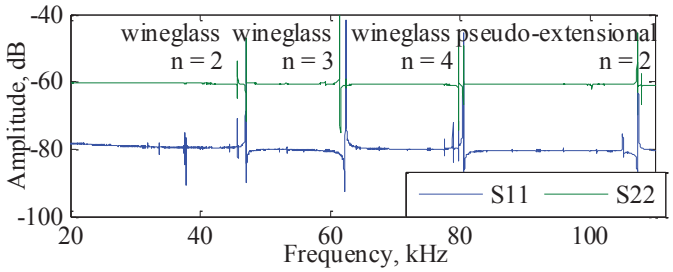

Fig. 5. Frequency sweep of vibratory modes showing wineglass n = 2, n = 3, and n = 4 modes followed by pseudo-extensional n = 2 mode.

Table I: Composite ring parameters.

Device diameter (mm)	1.78
Device layer thickness (μm)	40
Capacitive gaps (μm)	1.5
Individual ring width (μm)	5
Number of individual rings	40

Table II: Wineglass vs. extensional mode.

	WG	PE
Modal mass (kg)	2.35e-8	2.25e-8
Angular gain k, ($0 < k \leq 1$)	0.76	0.78
Quality factor (measured)	160,000	109,000

arrangement in Fig. 3 [2,3]. Simultaneous operation of fundamental and higher order modes is possible [6] but outside of the scope of this paper. The fundamental mode is differential with respect to the electrodes, while the pseudo-extensional mode is seen as common-mode with respect to the electrodes. Fig. 3 shows the configuration for excitation of the PE mode only. A differential-gap change, such as induced by temperature/stress or linear vibration, will impact sensitivity of rate (and offset) of a gyroscope operated in the WG mode. The PE mode, in contrast, is less sensitive to differential-gap change (because the electrodes configuration, Fig. 3, is more sensitive to a common-mode gap change) which in turns makes this mode less sensitive to shock/vibrations and hence ideal for applications with harsh, high-G environments.

C. Modal Analysis

Fig. 2 and Table II show the results of FEA simulation of the device presented in Fig. 1. Modal displacements and vibrational energy distribution for wineglass and pseudo-extensional is shown in Fig. 2 (anchors and suspension omitted for clarity but considered in simulation). The modal mass was extracted from the eigenfrequency analysis by taking a ratio of the kinetic energy to the square of average velocity for each mode. The angular gain was calculated using the frequency domain analysis by harmonically driving the PE mode near its resonant frequency and extracting the amplitude of the degenerate PE mode in response to the applied rotation. As expected, the angular gain and the modal mass of pseudo-extensional n = 2 mode is the same as that of wineglass n = 2 mode, Table II. The innovative support system [3] ensures that the vibrational energy is spread across the composite ring width as opposed to traditional designs such as DRG [4] or TRG [5] where maximal energy is located either at the inner- or outermost ring. This, in turn, allows to maximize number of rings that participate in a vibratory motion and increase an angular gain to 0.8, close to theoretical limit of 1.

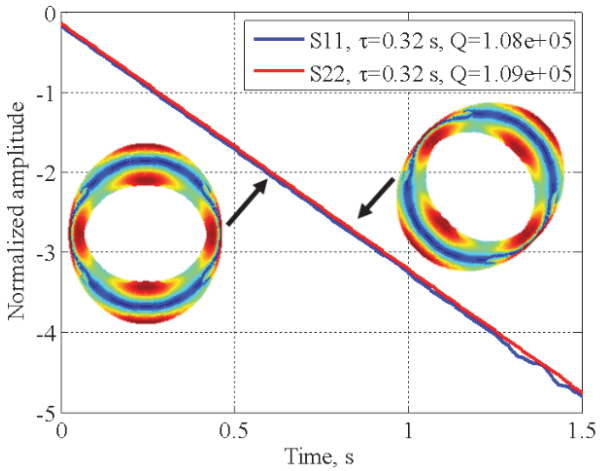

Fig. 6. Log-linear plot of ring down showing Q-factors of 108k and 109k for pseudo-extensional degenerate modes (S11 is drive-mode, S22 is sense-mode).

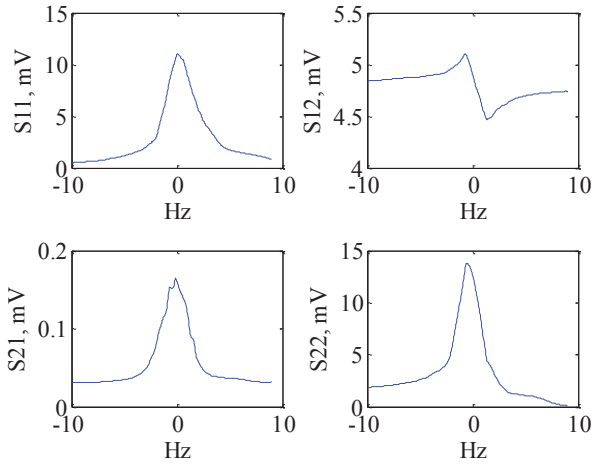

Fig. 7. Amplitude response after frequency (on-axis) and quadrature (off-axis) tuning. S11 is drive-mode, S22 is sense-mode, S12 and S21 are drive-mode and sense-mode quadrature, respectively. The S21 measure was made single ended.

D. Angular Gain

This section describes angular gain simulation in COMSOL. The resonator is harmonically excited at the frequency ω_d with forces applied to the electrodes in presence of rotation and a body load or rotating frame defined to create the Coriolis force. One complication for a ring-shaped gyroscope is that the electrodes sense the radial displacement which is not aligned with the material axis *u* and *v*. The radial displacement is along the direction of the surface normal in a ring gyroscope and can be extracted using the surface normal components as:

$$q_{1,2} = u \cdot solid.nX + v \cdot solid.nY$$

The Coriolis acceleration as we use it here is defined as:

$$\overline{a_c} = 2A_g \overline{\upsilon} \times \overline{\Omega},$$

where A_g is the angular gain, $\overline{\upsilon}$ is the velocity vector and $\overline{\Omega}$ is the rotation rate vector. For a rotation Ω_z around the *z*-axis, the acceleration is:

$$a_{cz} = 2A_g j\omega_d q_1 \Omega_z .$$

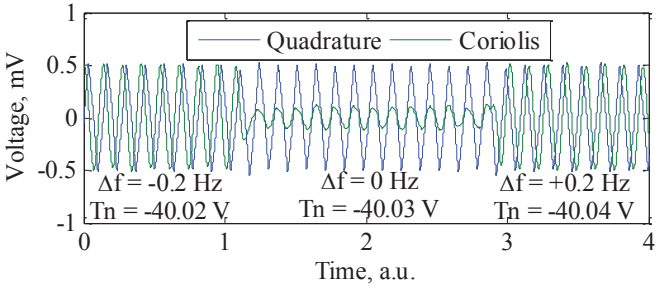

Fig. 8. Mode-matched operation is determined by applying a test signal to quadrature trim electrode. The demodulated Coriolis and Quadrature responses are in-phase and the Coriolis component is minimized when mode-matched as shown in this sweep over mode-matched and mode-split (±0.2 Hz) conditions.

Note the Coriolis acceleration is proportional to the velocity and the resulting displacement for a mode split gyroscope will be imaginary. The displacement for a given applied acceleration due to a rotation rate around the *z*-axis is:

$$\mathrm{Im}\{q_2\} = Q_{eff} a_{cz} / \omega^2 = 2A_g \omega_d q_1 \Omega_z Q_{eff} / \omega^2 ,$$

where ω is the modal frequency of the gyroscope sense mode and Q_{eff} is the modal gain, which for a simulation with effectively infinite Q is approximately:

$$Q_{eff} \approx 1 / \left(1 - (\omega_d / \omega)^2\right).$$

Choosing Q_{eff} in a 100-500 range allows the solver to converge easily while limiting any distortion in the mode shape from non-ideal forcing of the model. Solving for the angular gain:

$$A_g = \mathrm{Im}\{q_2\} \omega^2 / \left(Q_{eff} \omega_d q_1 \Omega_z\right).$$

For the pseudo-extensional mode gyroscope, the simulated angular gain is 0.8 while for the typical tuning fork gyroscopes the angular gain can approach the theoretical maximum of 1.

III. Experimental Results

A. Setup

Prototypes of pseudo-extensional mode ring gyroscopes were fabricated using a wafer-level, vacuum sealed Epitaxial Silicon Encapsulation "Hot Dog" process, Fig. 4. The 2×2 mm^2 die size devices were packaged in 28 pin LCC and mounted on a PCB with front-end electronics. All control and signal processing were realized using an HF2LI Zurich Instruments lock-in amplifier. Amplitude control, quadrature nulling, modulation, and mode-matching closed-loops were implemented on the Xilinx microcontroller μBlaze using the Real-Time Kit (RTK) of HF2LI as reported in [8].

B. Electrostatic Tuning

A DC bias voltage of 20 V and AC voltage of 20 mV were used for initial experimental characterization. Frequency sweep of the gyroscope revealed Wine Glass (WG) n = 2, n = 3, and n = 4 modes followed by Pseudo-Extensional (PE) n = 2 mode, Fig. 5, closely matching the eigenfrequency simulation (S11 and S22 are degenerate modes). Log-linear plot of ring down showed Q-factors of 108,000 and 109,000 for PE degenerate modes, Fig. 6. Prior to operation, the device was electrostatically trimmed to compensate for the fabrication imperfections. As-fabricated 500 Hz frequency split for PE mode is attributed to the single-crystal wafer orientation. For comparison, as-born

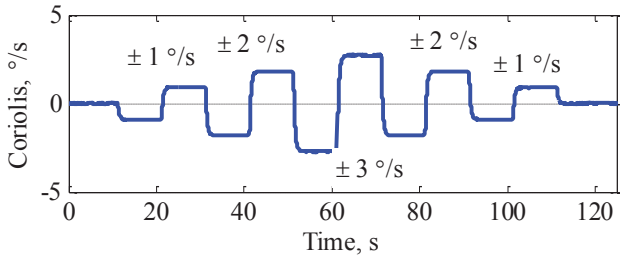

Fig. 9. Rate response demonstrating operation under ±1 to ±3 °/s inputs.

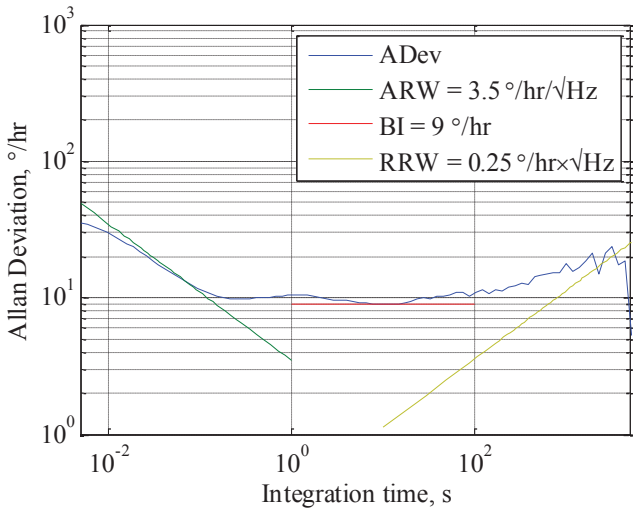

Fig. 10. Noise analysis revealed 9 °/hr in-run bias and 0.06 °/√hr ARW. The 1/f noise is due to a known setup issue (as seen from S12 in Fig. 7).

frequency split for WG modes could be as high as 10 kHz for 0.6 mm DRG with regular layout and as low as 100 Hz with modified spoke angles to compensate for wafer orientation [4]. The on-axis tuning electrodes ($T_{0°}$ and $T_{45°}$ in Fig. 4) were used to match the frequencies of the degenerate modes and off-axis tuning (Q^- and Q^+ in Fig. 4) to remove quadrature. The electrodes were designed to selectively tune the PE mode and reduce sensitivity to WG modes. This was accomplished by utilizing the $T_{0°}$ and $T_{45°}$ electrodes on the inside of the ring. Since the vibrational energy of the WG mode is located in the outermost ring, the inner electrodes were ineffective. In contrast, the energy of PE mode is concentrated on the opposite sides of a composite ring making it highly sensitive to the inner electrodes. The on-axis tuning sensitivity for PE mode was 0.15 Hz/V^2 (while negligible for WG mode) requiring 60 V DC potential to mode-match the gyroscope. Fig. 7 shows amplitude response after tuning: S11 plot is the drive-mode response, S22 is the sense-mode, S12 and S21 are drive-mode and sense-mode quadrature, respectively. The drive voltage was unintentionally made single ended resulting in feedthrough as evident from S12 quadrature measurement and compromising performance.

C. Control Loops and Active Mode-Tuning

The gyroscope was operated with conventional control loops including a phase locked loop, an amplitude control, and quadrature control [7]. In high Q-factor, mode-matched gyroscopes which are packaged at very low pressure, quadrature leakage and frequency mismatch can be the dominant offset sources. To mitigate these errors, a mode-matching loop continuously observes the frequency mismatch by dithering the quadrature trim voltage and adjusts the frequency mismatch by applying a tuning voltage to on-axis electrodes as described in [7]. To ensure that the PI controller for quadrature nulling did not interferey with the quadrature dither signal, the PI gains were chosen to set a quadrature loop bandwidth below the frequency of a modulation signal. Fig. 8 shows the tuning voltage sweep from –40.02 V to –40.04 V (relative to +20 V bias) to demonstrate gyroscope outputs at mode-matched and mode-split (±0.2 Hz) conditions. The rate response to quadrature dither is minimized when mode-matched.

D. Noise Performance

The noise performance of the PE mode was evaluated with control loops as described in the previous section. Rate response demonstrating operation under ±1 to ±3 °/s inputs shown in Fig. 9 confirms the gyroscope operation. The gyroscope was driven in linear regime. Allan deviation noise analysis of the zero rate output revealed 0.06 °/√hr Angle Random Walk (white noise), 9 °/hr in-run bias (1/f noise), and 0.25 °/hr×√Hz Rate Random Walk, Fig. 10. The 1/f noise and RRW are likely due to a known setup issue caused by an unintentional, non-differential drive (as evident from S12 plot in Fig. 7) resulting in feedthrough and the typically large 1/f noise of modulated drive DACs.

CONCLUSIONS

This work presents operation of the MEMS axisymmetric gyroscope in a higher order, ring width mode without compromising the angular gain. The device was operated in a pseudo-extensional mode with a similar angular gain as a conventional ring gyroscope of the same size/footprint operating in a wineglass mode. An advantage inherent to the extensional mode is the local rejection of linear accelerations as compared to the fundamental wineglass mode, which can only reject linear accelerations by matching electrodes across the diameter of the ring. Moreover, the inner and outer anchors supporting the ring not only traps the vibrational energy within the gyroscope and improves the Q-factor but also stiffens modes that are sensitive to external vibrations (e.g. translational modes) thereby reducing G-sensitivity and shock susceptibility. Initial characterization clearly demonstrates feasibility of using the pseudo-extensional mode of vibration for rate sensing with Q-factors of 110,000 and noise level of 0.06 °/√hr for a 2×2 mm^2 gyroscope.

REFERENCES

[1] http://www.siliconsensing.com/technology/evolution-of-vsg/
[2] S. Tallur, S. Bhave, “Compound Mode Gyroscope,” US Patent Application 20170074656, March 16, 2017.
[3] J. Gregory, I. Prikhodko, “Ring Gyroscope Structural Features,” US Patent Application 20160123735, May 5, 2016.
[4] Chae Hyuck Ahn et al., “Mode-Matching of Wineglass Mode Disk Resonator Gyroscope in (100) Single Crystal Silicon,” in Journal of Microelectromechanical Systems, vol.24, no.2, pp.343-350, April 2015.
[5] D. Senkal et al., “100K Q-factor toroidal ring gyroscope implemented in wafer-level epitaxial silicon encapsulation process,” IEEE MEMS 2014, San Francisco, CA, 2014, pp. 24-27.
[6] H. H. Ge, D. Kim and R. M’Closkey, “Simultaneous exploitation of the fundamental and higher order wineglass modes in a vibratory gyro,” IEEE International Symposium on Inertial Sensors and Systems (ISISS) Proceedings, Hapuna Beach, HI, 2015, pp. 1-4.
[7] I. P. Prikhodko et al., “Mode-matched MEMS Coriolis vibratory gyroscopes: Myth or reality?,” 2016 IEEE PLANS, Savannah, GA, pp. 1-4.